Ab initio study of structural and electronic properties of yttria-stabilized cubic zirconia

G. Stapper
Max-Planck-Institut für Festkörperforschung, Heisenbergstrasse 1, D-70569 Stuttgart, Germany

M. Bernasconi
Max-Planck-Institut für Festkörperforschung, Heisenbergstrasse 1, D-70569 Stuttgart, Germany and Istituto Nazionale per la Fisica della Materia and Dipartimento di Scienza dei Materiali, Universitá di Milano, Via Emanueli 15, I-20126 Milano, Italy

N. Nicoloso and M. Parrinello
Max-Planck-Institut für Festkörperforschung, Heisenbergstrasse 1, D-70569 Stuttgart, Germany
(Received 10 July 1998)

Ab initio calculations have been performed on the structural and electronic properties of pure zirconia and yttria-stabilized cubic zirconia (YSZ). We use the local-density approximation to the exchange and correlation energy functional. We expand the Kohn-Sham orbitals in plane waves and use norm-conserving fully separable pseudopotentials. We find, in agreement with experiments that the most stable phase at zero temperature and pressure is the monoclinic baddelyte structure which transforms under pressure in the brookite orthorhombic phase. We then study the properties of the YSZ cubic phase using a supercell of 96 atoms. This is a defective structure where oxygen vacancies and yttrium substitutional impurities play a major role. The pattern of relaxation around the defects is consistent with the most recent scattering data, as well as their relative interaction which leads to a next-nearest-neighbor attraction between vacancy and yttrium. The analysis of the electronic properties show that single occupied color centers F^+ are only marginally stable and decay into neutral, doubly occupied F centers and empty (doubly charged) vacancies. Therefore, we found that the F^+ center in YSZ is a negative Hubbard-*U* site.
[S0163-1829(99)03002-7]

I. INTRODUCTION

Zirconia (ZrO_2) is an important technological material. It is one of the best corrosion-resistant and refractive materials used in metallurgy and as a thermal barrier coating in engines.[1] The addition of aliovalent oxides such as CaO, MgO, and Y_2O_3 improves substantially its thermomechanical properties by stabilizing at low temperature the cubic phase[3] which in pure zirconia is stable only at high temperature [>2650 K (Ref. 2)]. Cubic stabilized zirconia (CSZ) has very high strength, toughness, and thermal-shock resistance.[1] Furthermore the addition of substitutional cation (Ca^{2+},Mg^{2+},Y^{3+}) induces the generation of oxygen vacancies for charge compensation which makes CSZ a fast ion conductor used in oxygen sensors,[4] oxygen pumps for partial pressure regulation,[5,1] and high-temperature fuel cells.[6] The amount of dopant necessary to stabilize the cubic phase is quite large. For instance, in yttria- (Y_2O_3) stabilized zirconia (YSZ), 8–40 % mol of yttria is required to stabilize the cubic phase.[7] At this high dopant concentration, the interaction between defects is believed to lead to complex ordering and aggregation of defects which have a crucial role in the ionic conductivity of CSZ. Despite extensive experimental studies[8–20] there is no clear description of the defect-defect interaction and aggregation, nor a clear understanding of the role played by impurities in the stabilization of the cubic phase. A great deal of work has been dedicated also to the study of the electronic properties of YSZ.[21–32,34,33,35] In fact, in order to improve the performances of YSZ as an ionic conductor, the characterization of the minority charge carriers is important as well. In particular the presence of oxygen vacancies in CSZ suggested the possible existence of color centers (F centers), as occurs in other better characterized metal oxides.[36–38] Experimentally, several deep electronic traps have been identified in the gap of YSZ but their assignment to well-defined intrinsic or extrinsic defect states is still controversial and no compelling evidence of the existence of F centers has been provided so far.

From the theoretical side, empirical shell models have been used to model CSZ stabilized by CaO (Ref. 39) and Y_2O_3.[40–42] However, later work showed that the shell model with only dipolar anion polarizability used by the previous authors is inadequate to describe the different phases of zirconia.[43] The partial covalent character of zirconia, outlined in many *ab initio* calculations,[44–48] is probably responsible for the difficulties encountered by empirical shell models which are instead successfully applied to other more ionic metal oxides. *Ab initio* methods have also been applied to the study of cation impurities and vacancies in cubic zirconia.[32,34,35,33] However, due to the small size of the model system used, the role of defect-defect interaction in the yttria-zirconia solid solution has been only partially addressed in these previous theoretical works.

In this paper we report on a first-principles study of the structural, electronic, and dynamical properties of yttria-stabilized zirconia in the density-functional theory (DFT) framework using Car-Parrinello simulations,[49,50] the computational details of which are reported in Sec. II below. We modeled YSZ doped with 14% mol of yttria by supercells containing up to 96 atoms, with the aim of identifying the

dopant-vacancy aggregation mechanism, the local structure of the yttria-zirconia solid solution and the role of defect-defect interaction in determining the local distortion with respect to the average cubic symmetry. In order to check the reliability of our theoretical framework for YSZ, we first computed the equation of state at zero temperature of several crystalline phases of pure zirconia (monoclinic, tetragonal, cubic, and brookite) and pure yttria. The calculated structural parameters, compressibility and transition pressures agree with experimental data within the usual accuracy of DFT calculations, as reported in Sec. III. Our work is an *ab initio* calculation which reproduces the correct hierarchy in energy of the various known crystalline phases of zirconia. In Sec. IV we report our results on the structural properties of YSZ. In particular we found that yttrium preferentially occupies the site next-nearest-neighbor (NNN) to the vacancy, in agreement with most recent experimental results[17,18] and in contrast with previous ones which suggested the site nearest neighbor (NN) to the vacancy.[15,16,13] We also found that the largest deviation from the ideal cubic symmetry is due to the displacement of oxygen atoms nearest neighbor to the vacancy which move mainly along $\langle 100 \rangle$, as proposed by most recent neutron-scattering measurements.[14] However, we also found that other oxygen atoms and metal cations can move substantially (as much as 0.2 Å). The complexity of the pattern of these latter minor displacements is probably the reason behind the diversity of the models deduced experimentally from the fitting of scattering data.

In Sec. V the calculated electronic structure of our YSZ sample is reported. Despite the presence of oxygen vacancies no electronic states in the gap corresponding to empty color centers are found in our model of stochiometric YSZ. In fact the Madelung field produced by the relaxed oxygen atoms NN to the vacancy prevents the formation of an empty electronic state in the gap. Conversely we found that two electrons can be trapped in a neutral F center that is 0.57 eV lower in energy than two single charged F^+ centers. Two F^+ centers are therefore unstable with respect to decay into an empty vacancy and a neutral F center. In turn the trapping of a single electron in an F^+ center is also only marginally favored (25 meV) with respect to electron injection in the conduction band. These results are consistent with experimental findings, but are in contrast with previous theoretical calculations[34,33,35] that neglected lattice relaxations. The deviation from ideal cubic symmetry is therefore crucial for the understanding of the electronic properties of YSZ.

II. COMPUTATIONAL METHOD

We adopted an *ab initio* DFT framework in the local-density approximation (LDA).[51] We computed the equation of state of the pure phases of zirconia by using norm-conserving *ab initio* pseudopotentials[52] and plane-wave expansion of Kohn-Sham orbitals up to a kinetic energy cutoff of 70 Ry. Integration over the Brillouin zone (BZ) was performed by using special points[53] in the irreducible part. Since the cation-oxygen half-distance in zirconia is very close to the outermost node of the $5s$ eletronic state of the cation we were forced to include as valence states the $4s$ and $4p$ electrons of yttrium and zirconium, in order to generate a ghost free, transferable pseudopotential. As shown in Ref. 54, the inclusion of the $4s$ and $4p$ states in the valence allows us to reproduce the bond length of the ZrO molecule, while by freezing the semicore $4s$ and $4p$ states the calculated ZrO bond length is 12% smaller.[55] The electronic configuration used for the generation of the zirconium pseudopotential was $[\mathrm{Ar}]4s^2 3d^{10} 4p^6 4d^2$ $(+2$ ion) and the core radii were 1.35, 1.45, and 1.55 a.u. for the *s*, *p*, and *d* wave functions, respectively. The electronic configuration for yttrium was $[\mathrm{Ar}]4s^2 3d^{10} 4p^6 4d^1$ $(+2$ ion) and the cutoff radii were 1.4, 1.4, and 1.59 a.u. The generated $5s$ pseudo-wave function does reproduce the outermost node of the corresponding all-electrons wave function. In the study of isolated defects in cubic ZrO_2 and of the YSZ we used a supercell containing 96 atoms with periodic boundary conditions. The lattice constant of YSZ was chosen according to the experimental relation $a = a_o + 0.003x$ where x is the mole percent of yttria and a_o is the extrapolated lattice constant of yttrium-free zirconia.[7] We chose a_o as our theoretical equilibrium lattice constant of cubic fluorite. In these latter calculations as well as in the study of pure yttria which contains 40 atoms in the unit cell, we restricted the BZ integration to the supercell Γ point. Moreover, a Vanderbilt ultrasoft pseudopotential[56] was used for oxygen, which allowed us to decrease the kinetic energy cutoff to 30 Ry in the supercell calculations. We checked that the geometrical structural parameters were converged within an error of 1% with the energy cutoff used. The optimization of the structure and the *ab initio* molecular-dynamics simulations in the supercell geometry were performed using the Car-Parrinello method.[49,50] Geometry optimization were performed using both a simulated annealing procedure and a Broyden-Fletcher-Goldfarb-Shanno algorithm.[57] In the Car-Parrinello molecular-dynamics simulations we used a time step of 0.24 fs and a fictitious electronic mass of 1050 a.u.

III. THE PURE ZIRCONIA AND YTTRIA PHASES

A. Y_2O_3

Yttria has a cubic structure of space group T_h^7 $(\mathrm{Ia}\bar{3})$.[58,59] The bravais lattice is body centered cubic and the conventional cubic unit cell contains 80 atoms. The unit cell contains two inequivalent cation sites, the sites $8a$ [8 yttrium atoms at positions $(\frac{1}{4},\frac{1}{4},\frac{1}{4})$] and $24d$ [24 atoms at position $(u,0,\frac{1}{4})$]. The oxygen atoms are at site $48e$ [48 oxygen atoms at position (x,y,z)]. The structure is thus defined by the lattice parameter a and by the four internal structural parameters x, y, z, and u.

We computed the equation of state of yttria at zero temperature by fully relaxing the internal structure at each volume in the body-centerd-cubic unit cell containing 40 atoms. Due to limited BZ sampling the equation of state had to be smoothed by correcting for the discontinuities in the basis set as a function of volume as described in Ref. 61. It was then interpolated by a Murnaghan function.[60] The calculated parameter of the Murnaghan equation of state and the internal structural parameters are compared in Table I with experimental data and previous *ab initio* calculations. The agreement with experimental data are within the usual accuracy of DFT-LDA calculations.

TABLE I. Theoretical and experimental structural parameters of Y_2O_3. B_0 is the bulk modulus at zero pressure and B_0' the derivative of B_0 with respect to pressure at zero pressure.

	a_0 (Å)	B_0 (GPa)	B_0'	$-u$	x	y	z
This work	10.483	143	3.9	0.0327	0.3905	0.1518	0.3803
Theor. Ref. 77	10.424	183	4.1				
Expt.	10.604 [a]	150 [b], 170 [c]		0.0327	0.3907	0.1520	0.3804 [a]

[a]Reference 59.
[b]Reference 78.
[c]Reference 79.

B. ZrO_2

Zirconia has three zero pressure phases. At low temperature the monoclinic ($C_{2h}^5, P2_1/c$) phase is stable.[62] Around 1400 K there is a phase transformation into the tetragonal ($D_{4h}^{15}, P4_2/nmc$) structure.[63,64] The tetragonal phase converts into the cubic fluorite phase ($O_h^5, Fm3m$) at 2650 K which in turn melts at 2950 K.[2,9] At high pressure a phase transition from monoclinic to the orthorhombic (orthoI) brookite phase ($Pbca$) is reported for pressure in the range 3–11 GPa.[65–68] Less consensus is achieved on the other structures found at higher pressure and temperature.[66,69,70]

We computed the equation of state of the monoclinic, tetragonal, fluorite, and brookite structures at zero temperature. In the BZ integration we used up to 10, 18, 44, and 8 special points in the irreducible part for monoclinic, tetragonal, fluorite, and brookite phases, respectively. The total energy of the different phases are converged within 2 meV/atom with respect to BZ sampling. The internal structure was optimized at each volume while the cell parameters were kept fixed at the experimental equilibrium values, except for the simplest tetragonal structure for which also the c/a ratio was optimized. This restriction is a minor approximation: in the monoclinic phase, for instance, the measured b/a and c/a ratio change by less than 1% and the β angle by 2.5° in the range of densities considered in our calculated equation of state.[65] The calculated energy versus volume data, fitted by a Murnaghan equation of state,[60] are reported in Fig. 1. The minimum energy of the different phases are compared in Table II with the results of previous *ab initio* calculations. At variance with previous works, the monoclinic phase is the lowest energy structure in agreement with experimental findings. To our knowledge our work is the first parameter-free calculation which reproduces the correct hierarchy in energy of the different phases. A previous *ab initio* calculation[71] within the same framework as that used here, except for the choice of a pseudopotential of zirconium, which did not include semicore states in the valence, failed to reproduce the correct energy hierarchy. The calculated transition pressure from monoclinic to brookite phase is 5.7 GPa, which compares well with the experimental transition pressure in the range 3–11 GPa.[72] The parameters of the calculated Murnaghan equations of state are compared in Table III with experimental data and previous *ab initio* calculations. The measured bulk modulus of the monoclinic phase is scattered in a wide range of 95–189 GPa. Uncertainties are also present in the measured bulk modulii (Table III) of the tetragonal and cubic phases, which are obtained at low temperature from yttria-stabilized phases and extrapolated to the zero impurity concentration limit. The theoretical internal structural parameters of the monoclinic and brookite phases are compared with the experimental data in Table IV. The only internal structural parameter of the tetragonal phase is the parameter z of the oxygen position $4d$ $(0,\frac{1}{2},z)$.[63] We follow the literature convention[44] of reporting the parameter $d_z = 0.25 - z$. The calculated c/a ratio and internal parameter d_z of the tetragonal phase as a function of volume are reported in Fig. 2. At the experimental equilibrium volume

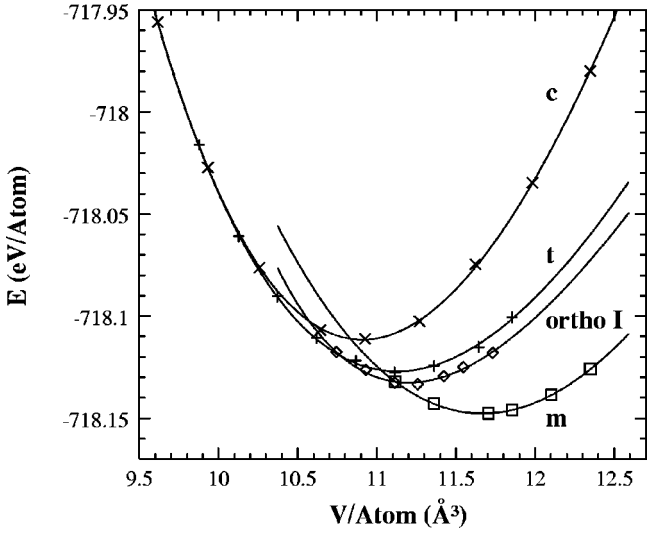

FIG. 1. Computed energy versus volume data fitted by a Murnaghan equation of state for monoclinic (m), tetragonal (t), cubic (c), and orthorhombic brookite (orthoI) phases.

TABLE II. Energies (eV/atom) at the minimum of the different phases with respect to the ground-state energy of the monoclinic phase. The experimental data for tetragonal corresponds to the enthalpy difference at the phase-transition temperature. The experimental data for cubic is obtained from the sum of the enthalpy differences at the monoclinic-tetragonal and tetragonal-cubic phase boundaries.

Tetrag.	Cubic	OrthoI	
0.021	0.037	0.013	This work
−0.005	−0.002		HF Ref. 32
0.048	0.015	−0.033	DFT Ref. 71
0.021	0.040		Expt. Refs. 80,81

TABLE III. Structural parameters of monoclinic, tetragonal, cubic, and orthorhombic brookite (orthoI) phases of zirconia. Our results are compared with experimental data and with previous Hartree-Fock (HF) and density-functional-based (DFT) *ab initio* calculations. The structural parameters of the orthoI phase corresponds to the volume at which the monoclinic → orthoI phase transition takes place.

Phase		V/Atom Å^3	B_0 GPa	B_0'
Cubic				
	This work	10.91	268	3.6
	Expt.	10.99 [a]	194–220 [b]	
	Theor. HF [c]	11.41		
	Theor. DFT [d]	11.34	267	
	Theor. FLAPW [e]	10.76	221	
Tetragonal				
	This work	11.13	197	5.0
	Expt.	11.02 [a]	190 [f]	
	Theor. HF [c]	11.45		
	Theor. DFT [d]	11.83	200	
	Theor. FLAPW [e]	10.81		
Monoclinic				
	This work	11.68	185	1.8
	Expt.	11.74 [f]	95–189 [g]	4–5 [h]
	Theor. HF [c]	12.28		
	Theor. DFT [d]	11.88	157	
Ortho I				
	This work	11.20	224	9.3
	Expt. [i]	11.23	181–281	4.2–5

[a]Reference 32, extrapolation to zero temperature using thermal-expansion data from Ref. 64.
[b]References 64, 1, 82, and 83.
[c]Reference 32.
[d]Reference 71.
[e]Reference 45.
[f]Reference 84.
[g]Reference 9.
[h]Reference 65, 85, and 86.
[i]References 68 and 69.

$c/a=1.435$ and $d_z=0.042$, which have to be compared with the experimental values $c/a=1.426$ and $d_z=0.0574$ obtained from extrapolation at zero temperature of the high-temperature measurements using thermal expansion data.[64] At the theoretical equilibrium volume $c/a=1.438$ and $d_z=0.044$.

The calculated structural parameters are overall in excellent agreement with experimental data and similar to the results of previous Hartree-Fock[44,32] and DFT (Refs. 45 and 71) *ab initio* calculations. As opposed to previous theoretical works our results also reproduce the correct relative energies of the different phases.

IV. YTTRIA-STABILIZED CUBIC ZIRCONIA

The fluorite phase of ZrO_2 can be stabilized at ambient conditions by doping with oxides like Y_2O_3. The dopant cations are believed to substitute for Zr^{4+} ions in the cation sublattice thereby creating, for charge compensation, one oxygen vacancy every two trivalent Y^{3+}. A simple rationalization of the stabilization process relies on the fact that the covalent nature of the Zr-O bond favors a sevenfold coordination of zirconium as in the monoclinic phase. The presence of oxygen vacancies in YSZ reduces the average zirconium coordination number from eight in the perfect fluorite to a value closer to seven. However, several factors may influence the stabilization process, such as defect-defect interactions in the solid solution.[32] Despite extensive experimental and theoretical work, so far no detailed quantitative description of the stabilization mechanism has been provided for. A first step towards the comprehension of the stabilization mechanism is the knowledge of the local environment of the dopant cations and vacancies in the solid solution. Since yttrium and vacancy can be seen as point defects with charge -1 and $+2$, respectively, Coulomb energy considerations suggest that yttrium is most likely nearest-neighbor (NN) to the vacancy. On the other hand, the aforementioned stabilization mechanism would maximize the number of seven-fold zirconium, leaving zirconium nearest neighbors to vacancies and yttrium next-nearest neighbor (NNN). Secondly, yttrium being an oversized cation would prefer an eightfold oxygen coordination. Experimental data disagree on the relaxation pattern around the defects, on the relative location of the dopant cations and vacancies and on the extent of vacancy-vacancy aggregation. Several extended x-ray absorption fine structure (EXAFS),[15] internal friction,[16] and neutron-diffraction[13] studies concluded that yttrium is NN to the vacancy, while other EXAFS (Refs. 17 and 18) data suggested that yttrium is NNN to the vacancy. Calculations with empirical potentials agreed with the latter model.[42] Concerning the deviation from the average cubic symmetry in the solid solution, several authors concluded from x-ray and neutron-diffraction measurements[8,10,9] that each oxygen site in YSZ can be replaced by four equivalent sites displaced along the $\langle 111\rangle$ directions. Contrary to this view other authors[12,11] proposed a model where the oxygen atoms NN to vacancies relax along the $\langle 100\rangle$ directions towards the vacancy. Steele and Fender[13] and Argyriou *et al.*[14] took this latter view from neutron-diffraction measurements, but allowed for a minority of oxygen atoms displaced along the $\langle 111\rangle$ directions. Moreover from neutron and x ray diffuse scattering several authors concluded that the oxygen vacancies are not randomly distributed on the anionic sublattice of cubic zirconia but they are strongly correlated (see Ref. 19 and references therein). However no consensus on a single model of vacancy correlation has emerged so far. For instance, models with vacancies preferably linked by $3^{1/2}a/2$ along $\langle 111\rangle$,[20] or with vacancies preferentially separated by a along $\langle 100\rangle$ or by $10^{1/2}a/2$ along $\langle 310\rangle$[19] (a is the lattice constant of cubic zirconia), have been proposed. As discussed in Sec. IV B, we addressed these issues by optimizing the structure of several YSZ configurations with 14% mol yttria content, well inside the region of stability of the cubic phase. Firstly, we present in the next section the preliminary calculations on the properties of dopant cation and vacancy at very low concentration limit which would represent the behavior of noninteracting defects. These calculations provide information on the local distortion around the defects

TABLE IV. Theoretical and experimental internal structural parameters in the Wyckoff notation (Ref. 87) for monoclinic and orthoI phases of zirconia. The theoretical data correspond to the experimental equilibrium volume.

		Wyckoff coordinates	
		This work	Expt.
Baddeleyite			
	$a=5.1505$ [a]	Zr(0.2769,0.0430,0.2100)	(0.2754,0.0395,0.2083) [a]
	$b/a=1.1012$	O_I(0.0640,0.3237,0.3524)	(0.0700,0.3317,0.3447)
	c/a=1.0234	O_{II}(0.4497,0.7560,0.4790)	(0.4496,0.7569,0.4792)
	$\beta=99.23°$		
OrthoI			
	$a=10.0861$ [b]	Zr(0.8848,0.0357,0.2531)	(0.8843,0.0332,0.2558) [b]
	$b/a=0.5217$	O_I(0.7895,0.3740,0.1268)	(0.7911,0.3713,0.1310)
	$c/a=0.0505$	O_{II}(0.9779,0.7393,0.4989)	(0.9779,0.7477,0.4948)

[a]Reference 9.
[b]Reference 88.

and a first estimate of the energy of vacancy-dopant aggregation. Moreover the comparison of the local distortion around the isolated defects with respect to the displacement pattern in the solid solution at higher dopant content will allow us to estimate the extent of defect-defect interaction.

A. Isolated defects

We relaxed a cubic supercell containing 96 atoms initially in the fluorite structure and either a substitutional yttrium, a vacancy (O^{2-} ion missing) or a vacancy-yttrium complex with yttrium NN or NNN to the vacancy. At this low dopant concentration (3.2% mol yttria) the cubic phase is unstable even locally. Therefore we fixed the positions of the atoms whose distance from a vacancy and an yttrium ion is larger than $\sqrt{3}a/2$ and $3a/4$, respectively.

The eight oxygen atoms NN to the isolated yttrium relaxed outwards along the $\langle 111\rangle$ directions by 0.09 Å, as required by the longer Y-O bond (2.25-2.34 Å in Y_2O_3) with respect to the Zr-O bond (1.89 Å). The zirconium atoms nearest to yttrium relax towards the dopant by 0.08 Å.

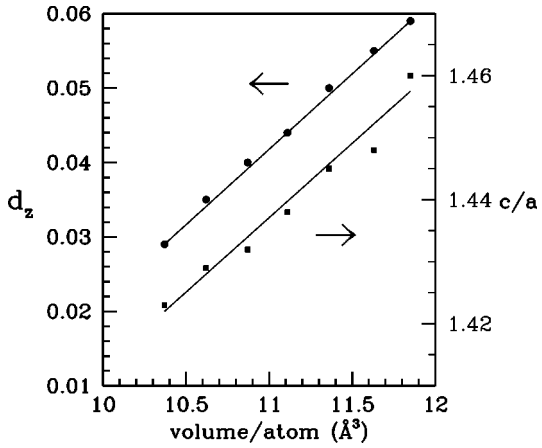

FIG. 2. Calculated lattice parameters ratio c/a and internal structural parameter d_z of the tetragonal phase as a function of volume.

The displacement pattern around an isolated oxygen vacancy (in the 95 atom supercell) is reported in Fig. 3. The oxygen atoms NN to the vacancy move towards it (0.24 Å) while the nearest zirconium atoms move outwards along the $\langle 111\rangle$ directions (0.18 Å), as expected due to repulsion from the +2 charged vacancy. The oxygen atoms nearest to the zirconium, but not NN to the vacancy, follow the displacement of the cation and move outwards along $\langle 111\rangle$ (0.04 Å). The oxygen atoms in the outermost right corner in Fig. 3 move inwards (0.04 Å) along $\langle 111\rangle$ not being dragged by any cation.

The displacement patterns of the complexes yttrium-vacancy with yttrium NNN or NN to the vacancy are reported in Figs. 4 and 5, respectively. In the configuration with yttrium NNN, the displacement pattern around the vacancy is only slightly modified by the presence of the dopant with respect to the isolated vacancy configuration in Fig. 3. The main perturbation is an enhancement of the displace-

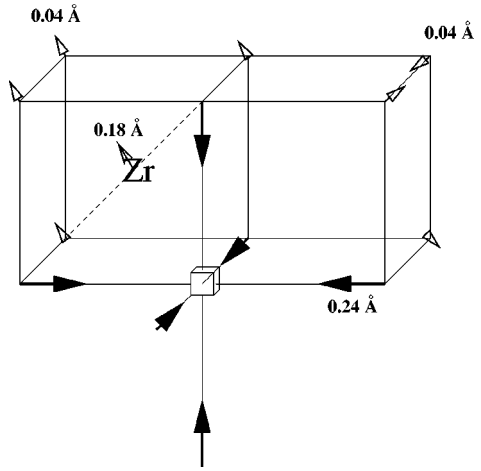

FIG. 3. Displacement pattern of atoms around an isolated vacancy in a 95 atom supercell. The vacancy is depicted as a small cube. Oxygen atoms occupy the sites at the corners of the cubes. Metal cations occupy half of the sites at the center of the cubes. The six oxygen atoms nearest neighbors to the vacancy move along $\langle 100\rangle$ while the zirconium atoms move outward along $\langle 111\rangle$.

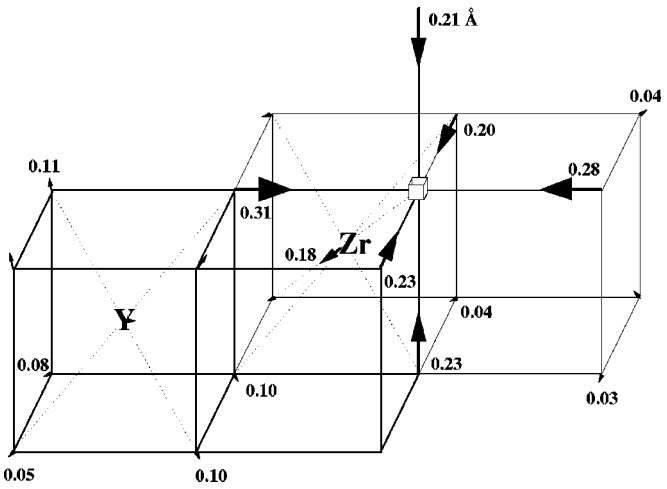

FIG. 4. Displacement pattern of atoms around an yttrium-vacancy complex with the yttrium next-nearest neighbor to the vacancy in a 95 atom supercell.

ment along ⟨100⟩ of one oxygen atom (0.31 Å) due to the superposition of vacancy attraction and yttrium repulsion. Conversely the presence of yttrium NN to the vacancy induces large changes in the displacement pattern with respect to the simple superposition of the isolated yttrium and isolated vacancy displacement patterns. In particular the displacement of the two oxygen atoms NN to both the vacancy and yttrium is drastically reduced, due to the opposite effects of vacancy attraction and yttrium repulsion. Moreover the yttrium atom moves outward with respect to the vacancy by nearly the same amount (0.12 Å) as zirconium does.

We estimated the yttrium-vacancy binding energy in the NN and NNN configuration as

$$E_{\text{bind}}=E^{\text{Y+vac}}-E^{\text{vac}}-E^{\text{Y}}-E^{\text{ZrO}_2},$$

where $E^{\text{Y+vac}}$ is the total energy of the supercell containing the yttrium-vacancy complex, E^{vac} and E^{Y} are the total energies of the supercells with isolated yttrium and vacancy, respectively, and E^{ZrO_2} is the energy per formula unit of the 96 atom supercell of ideal cubic zirconia. Since the defects are charged, the long-range cubic interaction between the

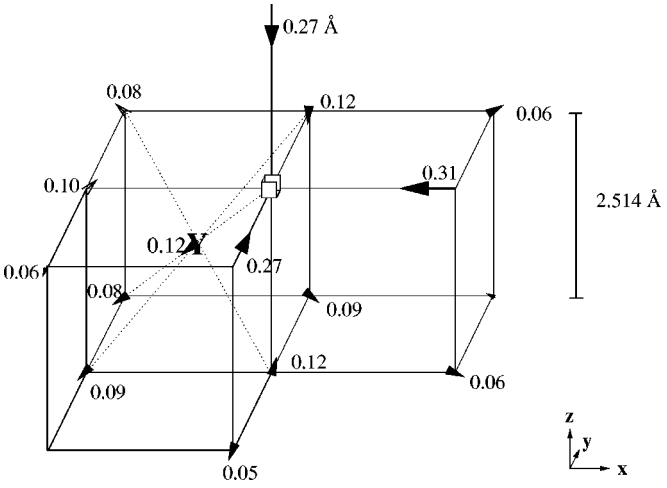

FIG. 5. The same as Fig. 4 for the yttrium nearest neighbor to the vacancy.

defect and its periodic images in the supercell calculations must be subtracted from the total energy. In the supercell calculations the system is neutralized by a uniform background as usual. The long-range defect-image interaction of isolated yttrium and vacancy is modeled as[73]

$$E_c=-\frac{1}{2}\alpha q^2/\epsilon_o L, \tag{1}$$

where $\alpha=2.6373$ is the Madelung constant for a simple cubic lattice, L is the lattice constant of the cubic supercell, and q is the charge of the defect (-1 for yttrium and $+2$ for the vacancy). $\epsilon_o=29.3$ is the estimated dielectric constant of YSZ.[39] The obvious generalization of the previous formula for the defect-image Coulomb interaction is used for the yttrium-vacancy complexes. E_{bind} is -0.44 eV and -0.10 eV for yttrium in the sites NNN and NN to the vacancy, respectively.

The behavior of isolated defects here described allow us to draw a preliminary comparison with the different structural models of YSZ proposed in the literature. First, the site NNN to vacancy is favored for yttrium by 0.34 eV with respect to the NN site. Secondly, in agreement with the most recent neutron-diffraction data[14] the main distortion from cubic symmetry is due to the displacement of the oxygen atoms NN to the vacancy. They move along ⟨100⟩ directions towards the vacancy by $\sim 0.2-0.3$ Å (exp. 0.17–0.23 Å, depending on the yttrium content[14]). In addition a large outwards displacement (0.18 Å) along ⟨111⟩ is found for cations NN to the vacancy. Cation displacement along ⟨111⟩ has been proposed by Steele and Fender[13] based on neutron-diffraction data and by Li *et al.*[18] from EXAFS. However, these authors assumed a cation displacement towards the vacancy which is opposite to what we found for both zirconium and yttrium. In particular yttrium may be expected to move towards the vacancy, being a -1 defect attracted by a $+2$ charged vacancy. Apparently this naive model of dopant-vacancy interaction is not adequate, as implied also by the fact that yttrium prefers the site NNN to the vacancy.

These main qualitative features of the local structure and energetics of defects in YSZ obtained here from the isolated defect calculations are confirmed by the more realistic calculations on the solid solutions at higher dopant concentration reported in the next section.

B. Solid solution

At normal conditions the fluorite solid solution is stable for yttria content in the range 8–40 % mol.[7] At lower yttria content the system is inhomogeneous and for yttria content higher than 40% mol the system crystallizes in the $Y_4Zr_3O_{12}$ ordered compound.[7] Besides experimental limitations, uncertainties are present in the precise location of the phase boundaries also because it is not fully established that the yttria-stabilized phases studied at normal conditions are thermodynamically stable and not simply metastable structures whose properties depend on the preparation conditions. Mixtures of cubic solid solution and segregated microdomains of $Y_4Zr_3O_{12}$ have also been proposed for yttria content between 15 and 40 % mol.[7]

We studied the properties of YSZ at 14.3% mol yttria, well inside the stability field of the cubic phase, by optimiz-

TABLE V. Configuration of defects in the different samples studied. $N^{\square\text{-}\square}$ is the number of vacancy-vacancy pairs with a given vacancy-vacancy distance. The distances are given as integers which correspond to the order of shells of neighbors in the appropriate sublattice. For instance the distance 4 for the vacancy-vacancy is the fourth shell of neighbors of the oxygen in the oxygen atom sublattice which correspond to the site reached by the vector $\langle 210\rangle a/2$. a is the lattice constant of cubic zirconia. Analogously $N^{\square\text{-Y}}$ and $N^{\text{Y-Y}}$ refer to vacancy-yttrium and yttrium-yttrium correlations. The pairs reported in the table are formed by a defect inside the supercell and by all the other defects in the crystal including the periodic images. Due to periodic boundary conditions the number of pairs is much larger than that obtained from the pair of defects both inside the supercell. The samples are classified in three sets: A, B, C (see text). The total energies of the relaxed structures are compared with the Coulomb energies of the unrelaxed structures obtained by assigning charges -1 to yttrium and $+2$ to vacancies.

Conf.	$N^{\square\text{-}\square}$					$N^{\square\text{-Y}}$			$N^{\text{Y-Y}}$				$E^{\text{relaxed}}_{ab\ initio}$	$E^{\text{ideal}}_{\text{Coulomb}}$
	$\square$-$\square$ distance					$\square$-Y distance			Y-Y distance					
	4	5	6	7	8	1	2	3	4	1	2	3	4	eV/Atom	eV/Atom
A0		4	1				16	13	3	7	6	16	2	−711.959	−42.121
A1		4	1			2	16	10	4	9		14	5	−711.963	−42.160
A2		4	1			1	16	11	4	7	4	16	3	−711.961	−42.149
A3		4	1			2	16	10	4	8	4	12	5	−711.960	−42.153
A4		4	1			2	16	10	4	10		14	4	−711.960	−42.160
B1		4	1			3	15	10	4	9	4	14	2	−711.956	−42.136
B2		4	1			1	15	13	3	8	6	12	4	−711.955	−42.125
B3		4	1			1	14	13	4	8	8	12	4	−711.953	−42.123
B4		4	1			4	14	10	4	8	6	16	1	−711.950	−42.141
B5		4	1			6	12	9	5	10	6	13	2	−711.940	−42.136
B6		4	1			8	10	10	4	12	6	10	2	−711.933	−42.159
C1		2	2	1	1		20	7	5	9		14	5	−711.957	−42.205
C2			4	2			22	4	6	8	2	12	7	−711.955	−42.225
C3	1	2		1	1		16	14	2	6	8	17	1	−711.944	−42.201
C4	2			2			16		16	8	8	8	4	−711.934	−42.276
C5	2			2		8	8	8	8	8	8	8	4	−711.900	−42.202

ing the structure of 16 different supercell samples. Since YSZ is a disordered system, ideally one would like to determine the defect distribution by making use of statistical sampling methods such as Monte Carlo. However this would require very large system sizes, prohibitively expensive in an *ab initio* calculation. Therefore, we built a model of YSZ using as much as possible the information on defect interactions obtained in the previous section. We started from a 96 atom supercell of cubic zirconia and added four vacancies and eight substitutional yttrium atoms in different configurations, keeping the vacancies not too close to each other and yttrium atoms NNN or NN to the vacancies. The relative positions of vacancies and dopant cations in the different samples are reported in Table V. The total energies of the relaxed supercells are compared in Table V with the Coulomb energies of the unrelaxed structures computed by assigning charges to the defects only ($+2$ to vacancy and -1 to yttrium).[74] The samples in Table V of the sets labeled A and B have the same distribution of the vacancies, but different yttrium configurations. The samples A also have the same number of yttrium in sites NNN to the vacancies and differ amongst themselves because an yttrium can be at the same time NN to a vacancy and NNN to another, due to high dopant content and small cell size.

From the total energies of the different configurations in Table V we can infer defect-defect interaction energies. The first conclusions we can immediately draw is that there is no clear relation between the ideal Coulomb energies and the real total energies of the relaxed structures, indicating that atomic relaxation plays a crucial role. Secondly, by fixing the vacancy configuration the total energy decreases by increasing the number of yttrium atoms NNN to vacancies. In the configurations C3–C5 there are chains of vacancies aligned along $\langle 100\rangle$ at a distance of a. They are separated by an oxygen NN to two vacancies. Due to symmetry this central oxygen does not move and these configurations are energetically unfavorable. This result is in contrast with the model deduced from x-ray diffuse scattering[19] which assumes that the vacancies are preferentially joined by the vector $\langle 100\rangle a$. However, we must say that our vacancies aligned along $\langle 100\rangle$ are not a simple pair but an infinite chain, due to the finite size of our cell and the periodic boundary conditions.

In order to estimate the defect-defect aggregation energies in the solid solution we fitted the total energies as a sum of long-range screened Coulomb interaction between the defects plus the sum of two-body short-range potentials for vacancy-vacancy, yttrium-vacancy, and yttrium-yttrium interactions. The total energy is written as $E_{\text{tot}}=E_o+E_c+1/2\Sigma_{i,j}E_{\text{sr}}(r_{ij})$. E_o is a constant. The defect-defect interactions E_{sr} are short-range and defined for the distances r_{ij} between the defects in the ideal cubic sites. Above a given shell of neighbors the short-range interactions are set to zero. The long-range Coulomb interaction E_c is between $+2$ (vacancies) and -1 (yttrium) charges screened by the estimated dielectric constant of YSZ [$\epsilon_o=29.3$ (Ref. 39)]. This screened Coulomb potential also correctly describes the defect-image interaction.[73] In Table VI the short-range inter-

TABLE VI. Short-range interaction energies (eV) between defects fitted on the total energies of the 16 samples studied (see text). The distances between the defects are expressed as in Table V. □-Y + Coulomb in the last line is the sum of short-range and screened Coulomb potential interactions between vacancy and yttrium.

E_{sr} (eV)	Distance			
	1	2	3	4
□-Y	0.160	−0.299	−0.123	
Y-Y	0.123	0.208	0.025	
□-□	−0.730	−0.976	−0.560	−0.119
□-Y + Coulomb	−0.287	−0.532	−0.300	−0.149

action energies obtained from the fitting procedure are given. The total vacancy-yttrium interaction energy, $E_{sr}(r) - 2/\epsilon_o r$, as a function of yttrium-vacancy distance is given in the last line of Table VI. The yttrium-vacancy interaction potential has a minimum for yttrium NNN to the vacancy. The yttrium-vacancy aggregation energy is −0.29 and −0.53 eV for yttrium NN and NNN, respectively. The difference between the aggregation energies in the NN and NNN configurations (0.24 eV) is smaller but close to the value obtained from the isolated defects calculations in the previous section (0.34 eV). Similar values for vacancy-yttrium aggregation energy for yttrium NN [−0.4 eV,[40] −0.28 (Ref. 41)] and NNN (−0.39 eV)[42] to the vacancy have been obtained also from empirical shell-model calculations. The procedure of fitting the total energies as the sum of two-body potentials assumes that the interactions between the defects are additive which is in fact only a crude approximation since, as shown below, the displacement pattern in the solid solutions can show large deviation from the simple superposition of the displacement patterns of isolated defects. Nevertheless the parameters in Table VI provide a useful order of magnitude estimate of the defect-defect interaction energies. In particular the calculated yttrium-vacancy binding energy is in the range of values estimated from statistical models of vacancy unbinding and migration, fitted on ionic conductivity data as a function of temperature and dopant concentration.[75]

Regarding the structure of YSZ, the main local displacement pattern around the vacancy found in the isolated defect is preserved in the solid solution. In Tables VII and VIII the displacements of oxygen and metal cations are reported for the lowest energy samples of the sets A and B. For all the samples the largest displacement is for the oxygen atoms NN to the vacancies which move mainly along ⟨100⟩. In order to discuss in detail the structure of YSZ, we choose the sample A0 where no yttrium is NN to vacancies. Here all the oxygen atoms NN to vacancies (53% of the total number of O) move along ⟨100⟩ with displacement amplitude from 0.25 to 0.57 Å (average 0.34 Å, see Table VII), but for deviation in other directions smaller than 10%. The displacements of the oxygen atoms not NN to the vacancies are of different types: 25% of these O move less than 0.08 Å, another 25% move along ⟨111⟩ by ∼0.15 Å, another 25% move still along ⟨100⟩ by ∼0.15 Å and the rest move in different directions even as much as 0.2 Å. As in the isolated yttrium-vacancy complex studied in the previous section, most of the zirconium cations NN to the vacancies move outwards along ⟨111⟩ by ∼0.25 Å. However, some of the zirconium cations NN to the vacancies move still outwards but mainly along ⟨110⟩ by ∼0.25 Å. This happens when the zirconium is both NN to a vacancy and to an oxygen atom which is in turn NN to another vacancy in positions ⟨210⟩$a/2$ with respect to the first one. The zirconium is then repelled along ⟨111⟩ by the first vacancy, but attracted along ⟨001⟩ by the NN oxygen

TABLE VII. Displacements of oxygen atoms (Å) with respect to ideal cubic positions in the lowest energy samples of sets A and B (see Table V). Minimum, maximum, and average displacement are given separately for oxygen atoms NN and not NNN to vacancies. The average displacement over all oxygen atoms is given in the last column.

	O not NN to vac			O NN to vac			Total
Conf.	d_O^{min}	d_O^{max}	$\langle d_O \rangle$	d_O^{min}	d_O^{max}	$\langle d_O \rangle$	$\langle d_O \rangle$
A0	0.06	0.22	0.13	0.25	0.57	0.34	0.20
A1	0.05	0.30	0.15	0.07	0.83	0.34	0.20
A2	0.04	0.29	0.14	0.09	0.71	0.34	0.20
A3	0.03	0.34	0.14	0.08	0.84	0.34	0.20
A4	0.05	0.31	0.14	0.09	0.80	0.33	0.20
B1	0.05	0.33	0.15	0.18	0.70	0.33	0.20
B2	0.04	0.26	0.14	0.08	0.79	0.34	0.20
B3	0.05	0.28	0.14	0.18	0.69	0.34	0.20
B4	0.05	0.29	0.15	0.07	0.80	0.32	0.20
B5	0.03	0.26	0.15	0.07	0.65	0.29	0.20
B6	0.11	0.34	0.18	0.06	0.82	0.25	0.21

TABLE VIII. The same as in Table VII for metal cations.

	Not NN to vac.			NN to vac.			Total
Conf.	d_Y^{min}	d_Y^{max}	$\langle d_Y \rangle$	d_Y^{min}	d_Y^{max}	$\langle d_Y \rangle$	$\langle d_Y \rangle$
A0	0.07	0.11	0.09				0.09
A1	0.06	0.12	0.09	0.23	0.26	0.24	0.13
A2	0.05	0.13	0.09	0.23	0.23	0.23	0.11
A3	0.05	0.14	0.09	0.19	0.23	0.21	0.12
A4	0.04	0.13	0.09	0.21	0.26	0.24	0.12
B1	0.03	0.17	0.11	0.16	0.19	0.18	0.12
B2	0.07	0.13	0.09	0.19	0.19	0.19	0.11
B3	0.10	0.18	0.13	0.17	0.22	0.20	0.17
B4	0.02	0.13	0.09	0.18	0.22	0.20	0.15
B5	0.10	0.10	0.10	0.17	0.22	0.20	0.17
B6				0.16	0.25	0.21	0.21
Conf.	d_{Zr}^{min}	d_{Zr}^{max}	$\langle d_{Zr} \rangle$	d_{Zr}^{min}	d_{Zr}^{max}	$\langle d_{Zr} \rangle$	$\langle d_{Zr} \rangle$
A0	0.03	0.14	0.07	0.21	0.29	0.25	0.19
A1	0.04	0.21	0.09	0.21	0.29	0.24	0.18
A2	0.03	0.16	0.08	0.21	0.29	0.24	0.18
A3	0.02	0.21	0.07	0.21	0.29	0.24	0.17
A4	0.02	0.18	0.09	0.21	0.29	0.24	0.18
B1	0.03	0.17	0.09	0.20	0.33	0.26	0.18
B2	0.03	0.18	0.08	0.20	0.29	0.25	0.19
B3	0.01	0.10	0.07	0.20	0.30	0.25	0.14
B4	0.03	0.17	0.08	0.19	0.30	0.25	0.17
B5	0.01	0.10	0.07	0.20	0.30	0.25	0.14
B6	0.04	0.11	0.07	0.21	0.32	0.25	0.13

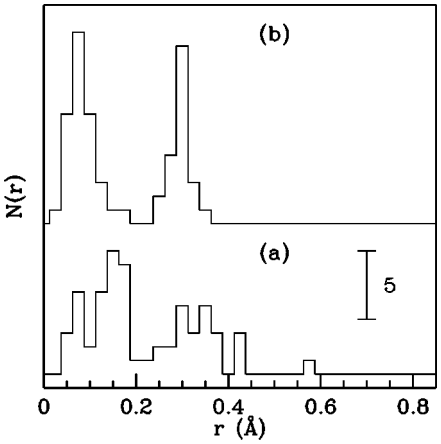

FIG. 6. Distribution of the oxygen atoms displacements with respect to ideal cubic positions in the YSZ sample A0 (see text) obtained from (a) full *ab initio* geometry optimization and (b) from linear superposition of the displacement patterns found for the isolated defects.

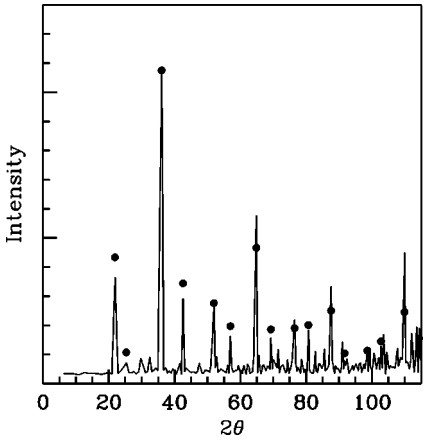

FIG. 7. Neutron-diffraction pattern computed from the molecular dynamics run of YSZ (ZrO_2-14.6 % Y_2O_3) at 315 K. The dots are the experimental scattering intensities of a sample ZrO_2-13% Y_2O_3 from Ref. 13. The theoretical diffraction pattern is computed by using the scattering lengths and neutron wavelength reported in Ref. 13. The theoretical structure factor is multiplied by the factor $1/\sin^2(\theta)\cos(\theta)$ to compare with experimental intensities. The largest peak is normalized to the experimental intensity.

which moves towards the second vacancy which results in a final displacement along $\langle 110 \rangle$. For the other samples where some yttrium atoms are NN to the vacancies, we found (as in the isolated defect calculations) that the oxygen NN to vacancies but not to yttrium have enhanced displacement mainly along $\langle 100 \rangle$ [here with deviation from $\langle 100 \rangle$ of up 20%]. Conversely the oxygen atoms NN to both yttrium and vacancies do not move appreciably. This is the reason for the small minimum and large maximum displacements of oxygen atoms NN to vacancies in Table VII for samples other than A0. A visual inspection of Fig. 6 reveals the extent of defect-defect interactions in determining the relaxation pattern of the solid solution. The figure reports the distribution of atomic displacement amplitudes in the relaxed sample A0, compared with what is expected from the linear superpositions of the isolated defects displacement patterns. Although the deviations from the linear superposition are usually large for the samples studied, the main pattern we identified from the isolated defects is still valuable and can discriminate between the different models obtained experimentally from scattering data. We can summarize our results as follows. The largest displacements occur for oxygen atoms NN to the vacancies which move mainly along $\langle 100 \rangle$. Although the average displacement amplitude (~ 0.3 Å) is close to that obtained in some models fitted on neutron-diffraction data [0.25–0.36 Å along $\langle 100 \rangle$ (Refs. 13, 12, and 14)], individual displacements can be as large as 0.6–0.8 Å (see Table VII). Besides oxygen NN to vacancies, other oxygen atoms can occasionally move as much as 0.2 Å in different directions. Only the metal cations NN to the vacancies move appreciably (~ 0.2 Å) outwards but not always along $\langle 111 \rangle$. The complexity of the pattern of these latter minor displacements is probably the reason behind the diversity of the models deduced by several groups analyzing scattering data.

In order to compare our structure with experimental data we computed the structure factor of sample A0 (including thermal effects) from a Car-Parrinello molecular-dynamics run at 315 K (1.3 ps long). Our results are compared in Fig. 7 with the experimental neutron-diffraction pattern on powders reported by Steele and Fender.[13] From the structure factor we computed the diffraction scattering intensity with the same nuclear scattering lengths and neutron wavelength used experimentally.[13] The diffraction patterns of the other samples of the set A are of similar quality. This shows that our samples do preserve on average a cubic arrangement as experimentally observed and gives us confidence on the reliability of the defects distribution chosen as a model of the solid solution.

From the molecular-dynamics trajectories we also computed the thermal mean-square displacement of the different species $\langle u^2 \rangle$ and the isotropic Debye-Waller factor $B = 8\pi^2 \langle u^2 \rangle$. The B factors for the different species are compared in Table IX with the experimental data. Our results are within the wide range of values reported experimentally. Another structural function, in principle, attainable from scattering data is the pair-correlation function. The calculated pair-correlation functions for the different species obtained from the molecular dynamics run at 315 K are reported in Figs. 8–11. The first peak of the Y-O pair-correlation function $g_{YO}(r)$ is at a greater distance with respect to $g_{ZrO}(r)$, as expected due to the longer Y-O bond. A clear signature of the distortion from ideal cubic structure is mostly evident in oxygen-oxygen $g_{OO}(r)$ (Fig. 8) and metal-metal $g_{MM}(r)$ (Fig. 11) pair-correlation functions. Both the total [Fig. 8(b)]

TABLE IX. Debye-Waller factor B (see text) computed from the molecular dynamics run at 315 K and from the experimental data of Refs. 13,12,14. O^{nn} and Zr^{nn} refer to quantities computed only for atoms NN to vacancies.

	B(Å^2)	
Atom	Expt.	This work
O^{nn}		1.45
O	0.63–1.2	1.26
Zr^{nn}		0.83
Zr,Y	0.62–1.43	0.95

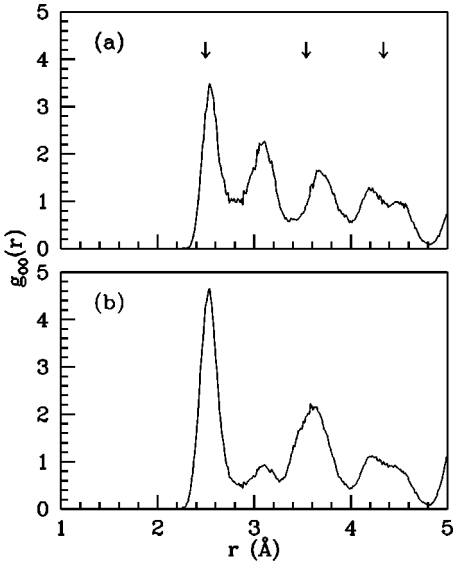

FIG. 8. Oxygen-oxygen pair-correlation function computed from the molecular dynamics run of YSZ at 315 K, 1.3 ps long for (a) the oxygen atoms nearest neighbors to the vacancies and (b) all the oxygen atoms in the sample. Arrows indicate the peaks position in the ideal cubic structure.

and partial [Fig. 8(a)] $g_{OO}(r)$, computed for the oxygen atoms only NN to the vacancies, show an additional peak at ~ 3.1 Å not present in the ideal fluorite structure. This peak is due to a pair of oxygen atoms which are both NN to the same vacancy. By relaxing towards the vacancy their separation decreases from the ideal 3.54 Å to 3.1 Å thus producing the additional peak in Fig. 8. In the metal-metal pair-correlation function (Fig. 11) the additional peak at ~ 3.9 Å is due to the displacement of zirconium atoms NN to the vacancies.

V. ELECTRONIC PROPERTIES OF YTTRIA-STABILIZED CUBIC ZIRCONIA

The measured optical band gap of the monoclinic and tetragonal phases of pure zirconia is around 5.2 eV.[76] DFT calculations of the electronic structure of pure zirconia[46,47] suggest that the electronic gap of the cubic phase should be

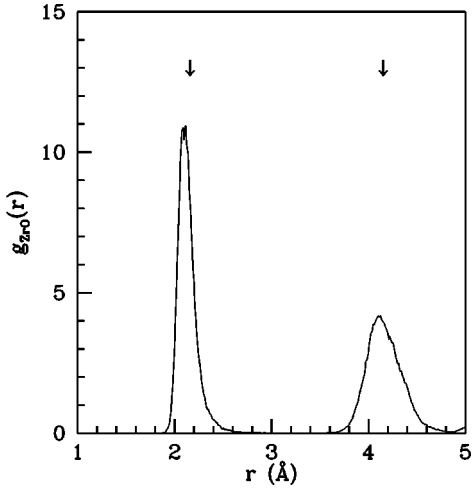

FIG. 9. Zirconium-oxygen pair-correlation function computed.

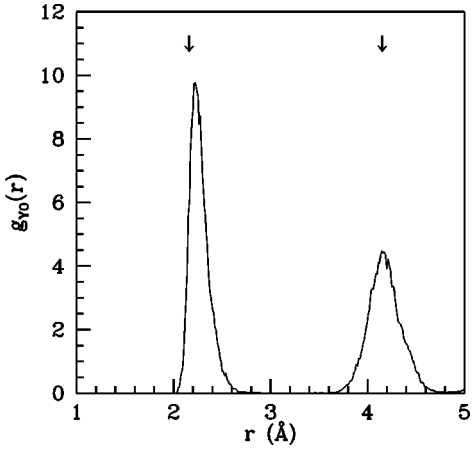

FIG. 10. Yttrium-oxygen pair-correlation function.

similar. In YSZ the true band gap between extended states in valence and conduction bands is estimated around 5.2–5.8 eV from absorption and photoluminescence spectroscopy.[22–24] However, a consistent absorption tail develops already around 4 eV.[21] This apparent absorption edge is attributed to transitions from the valence band to still unassigned localized states in the gap, either due to extrinsic defects or induced by the disorder in the yttria-zirconia solid solution.[25] The presence of oxygen vacancies in YSZ suggested the possibility of the formation of color centers (doubly charged vacancy with no trapped electrons, singly charged F^+ with one trapped electron and neutral F with two trapped electrons) as seen in other metal oxides such as MgO, CaO,[36,37] and SnO_2.[38] Color centers in different charge states were proposed by several authors[34,33,35] based on DFT calculations on clusters or supercell geometries. However, these latter calculations did not include consistently atomic relaxations whose amplitude in YSZ is so large around the vacancy that a quantitative result could hardly be drawn from electronic structure calculations which neglect them. Experimentally, deep electronic traps in the gap are detected in optical absorption and EPR measurements when additional electrons are added either by electron-hole generation in UV or x-ray-irradiated samples[27] or by reducing YSZ in low oxygen partial pressure atmosphere.[28,30] A broad absorption band centered at 365 nm (yellow color) appears upon irradiation[29] or reduction.[28,30] At higher electron content in heavily reduced samples, another broadband at 480 nm (dark brown color) is observed in absorption.[28,21,30] The

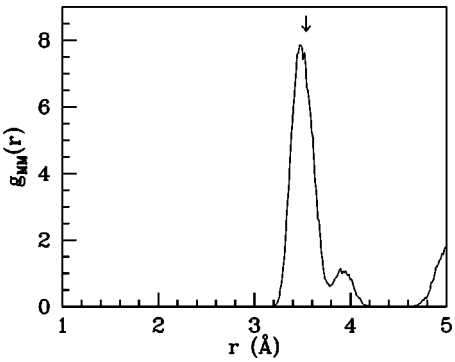

FIG. 11. Metal-metal pair-correlation function.

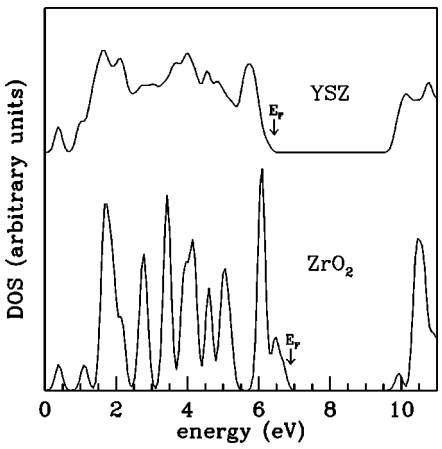

FIG. 12. Electronic density of state (DOS) of pure zirconia and YSZ (sample *A*0, see Sec. IV B), computed from the Kohn-Sham orbitals at the Γ point of the 96 atom supercells. DOS are broadened by a Gaussian with 0.1 eV variance. E_F is the Fermi level. The oxygen $2s$, zirconium and yttrium $4s$ and $4p$ states are below -10 eV.

yellow color center appears together with a paramagnetic EPR signal,[28,30,29] while the dark brown center is not EPR active. Although the 365 nm line was initially attributed to the F^+ center,[31] later analysis of the symmetry of the associated EPR signal argued in favor of a sixfold Zr^{3+} site[29,28] or to a seven-fold coordinated Ti^{3+} impurity.[26] On the other hand the 480 nm line has been attributed to a seven-fold coordinated Zr^{3+} ion.[28] Other authors,[30] based on the absence of EPR activity, assigned instead the latter line to a neutral F center and assumed that two single charged F^+ centers apparently not seen in EPR would eventually decay into the neutral, EPR inactive F center. However, a compelling experimental evidence of a color center in any charge state is still lacking.

Here we address this issue by computing the electronic structure of the samples described in the previous sections. In Fig. 12 the electronic density of states (DOS) of pure cubic zirconia and of the YSZ sample (A0) are compared. Since we used only the Γ point of the 96 atoms supercell, the DOS of the pure system appears as a series of peaks. In YSZ the doping and disorder broaden the peaks, but change the band gap only slightly from 3.3 eV in pure zirconia to 3.6 eV in YSZ (cf. Fig. 12). Previous DFT-LDA band-structure calculations[33,46,45,48] found a direct band gap in cubic zirconia in the range 3.3–4.1 eV, in agreement with our result. As apparent in Fig. 12 no electronic traps are present in the gap of YSZ. Although oxygen vacancies are present in the sample, the large inward relaxation of oxygen atoms NN to the vacancies generates a Madelung field which prevents the formation of a deep state in the gap associated with an electron trapped in the vacancy (color center). In order to further support this interpretation we computed the DOS for the isolated vacancy configuration described in Sec. IV A. In Fig. 13 the DOS of the isolated vacancy in relaxed and unrelaxed configurations in different charge states is reported. We adopted the local-spin density approximation (LSD) for the configurations containing an unpaired spin. The value of the band gap, the conduction band minimum (CBM), the valence band maximum (VBM), and the position of the color center level with respect to the VBM are reported in Table X for the different configurations of the vacancy. The energy gain due to atomic relaxation is also shown. The unrelaxed vacancy with charge $+2$ (no trapped electrons) does show the empty color center state in the gap [Fig. 13(a)] predicted by previous theoretical work.[33,35] However, the relaxation of the oxygen atoms NN to the vacancy shifts the color center level inside the conduction band and the empty electronic state in the gap disappears. If we add an electron to the unrelaxed vacancy a F^+ state is present in the gap [Fig. 13(b)]. The Madelung field produced by the relaxed oxygen atoms shifts the color center state to higher energy but still below the CBM in this latter case [Fig. 13(b)]. Due to the presence of the trapped electron in the F^+ center the oxygen atoms NN to the vacancy relax along $\langle 100 \rangle$ toward the vacancy by only 0.13 Å, compared with the displacement amplitude of 0.23 Å for the $+2$ charge state (see Sec. IV A). However, the total energy of the relaxed vacancy with one electron trapped in the F^+ center is only marginally lower (26 meV) than the energy of the fully relaxed vacancy (Fig. 3) with the additional electron injected in the conduction band. Therefore the ability of the vacancy to trap an electron in the F^+ state is marginal. Conversely, by adding two electrons to the vacancy a neutral F center is clearly found both in the unrelaxed and relaxed [Fig. 13(c)] configurations. With two electrons trapped in the vacancy the oxygen atoms relax along $\langle 100 \rangle$ by only 0.07 Å. The total energy of the neutral F center is such that two isolated F^+ centers are unstable with respect to decay into a doubly occupied F center and an empty vacancy. The energy gain U of this latter process is computed as $U=E_o+E_2-2E_1$, where E_0, E_1, and E_2 are the total energies of the relaxed F, F^+, and the doubly-charged-vacancy centers, respectively. We subtracted from the supercell total energy the Coulomb energy due to the interaction of the charged defects with their periodic images. The defect-image Coulomb energy is estimated by the formula (1) where q is $+2$ for the $+2$ charged vacancy and $+1$ for the F^+ state, and α, ϵ_o, and L are as before (see Sec. IV B). The resulting negative ''Hubbard-U'' of the color center is $U=-0.56$ eV. Our results support the assumption made in Ref. 30 that the F^+ center is unstable and even reproduce the numerical value of U used there[30] to model the defect concentration as a function of oxygen partial pressure in the reduced samples. In other metal oxides [MgO,[36] SnO_2 (Ref. 38)] where the F center exists for several charge states, the pure phase is stable and the oxygen atoms NN to a vacancy relax only slightly. Conversely the ideal cubic phase is unstable in pure zirconia at normal conditions. The cubic phase is stabilized only by the presence of vacancies and metal impurities in YSZ where the atoms NN to the vacancies have large relaxation and partially close the void of the vacancy, hindering the electron trapping. The oxygen atoms should move back closer to the ideal cubic positions to allow the localization of an electron in the vacancy. The energy gain due to electron trapping from the conduction band is opposed to an energy cost due to the outwards displacement of oxygen atoms. In the neutral F center the energy gain due to electron trapping is twice the trapping energy of a single electron in the F^+ (apart from on-site Coulomb repulsion) while the additional lattice energy cost is only slightly larger. This energy balance makes F^+ a negative Hubbard-U center.

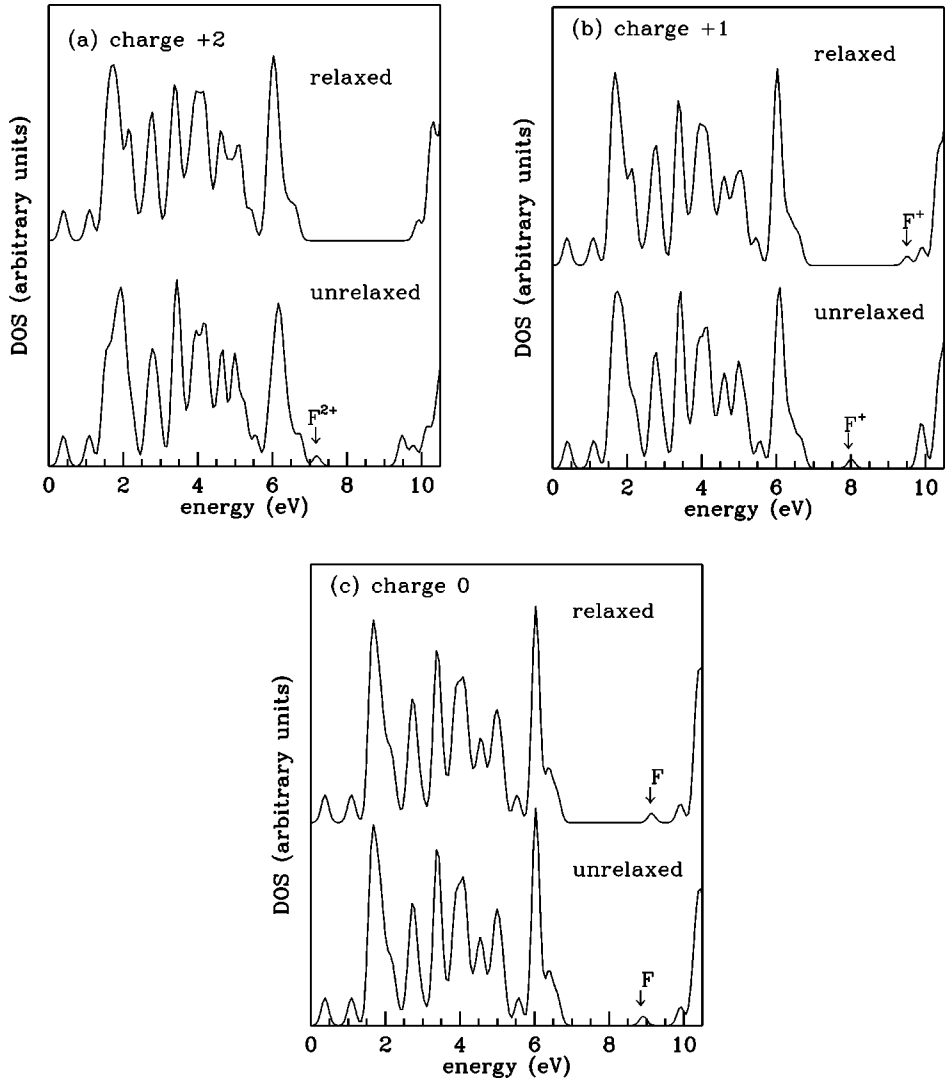

FIG. 13. Electronic density of state of an isolated vacancy in a 95 atom supercell in different charge states. DOS for relaxed and unrelaxed configurations are reported. (a) charge +2 (no trapped electrons); (b) charge +1 (one trapped electron); (c) charge 0 (two trapped electrons). The arrows show the position of the levels induced by the presence of the vacancy (color centers).

Since in YSZ the vacancies have a charge +2, compensated by the presence of substitutional yttrium, the additional electrons forming the F neutral centers must be provided by reducing the sample (adding additional neutral vacancies) or by electron-hole generation by irradiation. The DOS in Fig. 13 correspond to an isolated vacancy without yttrium impurity. As shown in Sec. IV A yttrium does not affect the oxygen displacement pattern around the vacancy when placed in the lowest energy site NNN to the vacancy. Since yttrium is a −1 charged defect, its presence close to the vacancy might be expected to produce an additional repulsive Madelung field for the electrons which would push up the energy of the F centers. However, by adding an additional electron and an yttrium impurity in the NNN site, we found that the position of neutral F center level with respect to the valence band maximum is only slightly lower in energy (0.02 eV) than the value reported in Table X. Although mainly localized in the vacancy region, the wave function of the electron trapped in the color centers has a not-negligible overlap with the $d_{3z^2-r^2}$ atomic orbitals localized on the four Zr ions NN to the vacancy. The mixing of an *s*-like state localized in the vacancy with the *d* states of the neighboring cations is not surprising. In fact, the states at the bottom of the conduction band in pure zirconia have mainly *d* character.[35,44]

As a final remark, it should be noted that the calculated position of the color center levels with respect to the CBM is

TABLE X. Energy gap (E_g), valence band maximum (E_{VBM}), conduction band minimum (E_{CBM}), position of the F center (E_{def}) with respect to E_{VBM} for the isolated vacancy in relaxed and unrelaxed configurations of different charge state. The calculations refer to a 95 atom supercell. Energies are in eV. ΔE_r is the energy gain due to atomic relaxation.

	Ideal			Relaxed		
Charge	+2	+1	0	+2	+1	0
E_g	2.75	3.23	3.31	3.29	3.30	3.31
E_{VBM}	6.73	6.66	6.60	6.61	6.60	6.59
E_{CBM}	9.48	9.89	9.91	9.90	9.90	9.90
E_{def}	0.46	1.35	2.31		2.91	2.55
ΔE_r				3.50	1.18	0.16

probably underestimated due to the error in the electronic gap, usual in DFT-LDA framework. On the other hand, the value of the Hubbard-U is reliable since it is obtained from the difference of total energies not affected by the failures of DFT-LDA in describing excited-state energies. Therefore, while we are confident in the prediction of the instability of the F^+ center with respect to decay into the neutral F center, the exact positions of the color centers level with respect to the CBM require more sophisticated calculation beyond DFT-LDA that are better able to describe the excited-state energies.

VI. CONCLUSIONS

In summary, we have been able to correctly reproduce the structural behavior of pure zirconia at zero temperature and low pressure. Our calculations allow us to identify the main pattern of the atomic relaxation in YSZ. Based on total-energy calculations we assign the position NNN to the vacancy as the preferential site for yttrium location. Our results also confirm the model of the displacement pattern from the ideal cubic symmetry deduced from the most recent scattering data.[14] The largest deviation from the ideal cubic geometry is due to the displacement of the oxygen atoms NN to the vacancies moving mainly along $\langle 100 \rangle$ by 0.3 Å on the average. However, other atoms can move as much as 0.2 Å. The structure factor and the Debye-Waller factor computed from the dynamical simulation are in good agreement with the experimental scattering data and provide further evidence of the reliability of our model for YSZ. Furthermore the analysis of the electronic properties let us identify the F^+ color center as a negative Hubbard-U site. Although we have not addressed the problem of the mechanism of vacancy diffusion in the fast-ion conductor regime, simulations of the kind here described might help clarify this issue as well. On the other hand, the size of our samples, although fairly large for an *ab initio* calculation, are still too small to properly address the other issue of vacancies aggregation and ordering proposed in some experimental works.[19,20] However, the *ab initio* data provided in this work could be used to tune new, more transferable, empirical potentials[43] able to address this latter problem via thousand-atoms simulations.

ACKNOWLEDGMENTS

Discussions with A. Paleari, M. Catti, and G. Pacchioni are gratefully acknowledged.

[1] *Science and Technology of Zirconia*, edited by A. Heuer and L. W. Hobbs, *Advances in Ceramics*, Vol. 3 (The American Ceramic Society, Westerville, OH, 1981); *Science and Technology of Zirconia II*, edited by A. Heuer and L. W. Hobbs, *Advances in Ceramics*, Vol. 12 (The American Ceramic Society, Westerville, OH, 1984).

[2] M. Yoshimura, Ceram. Bull. **67**, 1950 (1988).

[3] T. H. Etsell and S. N. Flengas, Chem. Rev. **70**, 339 (1970).

[4] W. J. Fleming, J. Electrochem. Soc. **124**, 21 (1977).

[5] C. B. Alcock, Mater. Sci. Res. **10**, 419 (1975).

[6] F. J. Rohr, in *Solid Electrolytes*, Material Science Series (Academic, New York, 1978), p. 431.

[7] C. Pascual and P. Durán, J. Am. Ceram. Soc. **66**, 22 (1983).

[8] R. E. Carter and W. L. Roth, in *EMF Measurements in High Temperature Systems*, edited by C. B. Alclock (The Institute of Mining Metallurgy, London, 1963).

[9] C. J. Howard, R. J. Hill, and B. E. Reichert, Acta Crystallogr., Sect. B: Struct. Sci. **44**, 116 (1988).

[10] H. Horiuchi, A. J. Schultz, P. C. W. Leung, and J. M. Williams, Acta Crystallogr., Sect. B: Struct. Sci. **40**, 367 (1984).

[11] J. Faber, M. H. Mueller, and B. R. Cooper, Phys. Rev. B **17**, 4884 (1978).

[12] M. Morinaga, F. Frey, and H. Schultz, Acta Crystallogr., Sect. A: Cryst. Phys., Diffr., Theor. Gen. Crystallogr. **36**, 520 (1979).

[13] D. Steele and B. E. F. Fender, J. Phys. C **7**, 1 (1974).

[14] D. N. Argyriou, M. M. Elcombe, and A. C. Larson, J. Phys. Chem. Solids **57**, 183 (1996).

[15] W. L. Roth, R. Wong, A. I. Goldman, E. Canova, Y. H. Kao, and B. Dunn, Solid State Ionics **18&19**, 1115 (1986); H. Morikawa, Y. Shimizugawa, F. Marumo, T. Harasawa, H. Ikawa, K. Tohji, and Y. Udagawa, J. Ceram. Soc. Jpn. **96**, 253 (1988); M. H. Tuilier, J. Dexpert-Ghys, H. Dexpert, and P. Lagarde, J. Solid State Chem. **69**, 153 (1987).

[16] M. Weller, Z. Metallkd. **84**, 6 (1993).

[17] C. R. A. Catlow, A. V. Chadwick, G. N. Greaves, and L. M. Moroney, J. Am. Ceram. Soc. **69**, 272 (1986); B. W. Veal, A. G. McKale, A. P. Paulinkas, S. J. Rothman, and L. J. Nowicki, Physica B **150**, 234 (1988); D. Komyoji, A. Yoshiasa, T. Moriga, S. Emura, F. Kanamaru, and K. Koto, Solid State Ionics **50**, 291 (1992).

[18] P. Li, W. Chen, and J. E. Penner-Hahn, Phys. Rev. B **48**, 10 063 (1993); **48**, 10 074 (1993); **48**, 10 082 (1993;); J. Am. Ceram. Soc. **77**, 118 (1994).

[19] Z. R. Dai, Z. L. Wang, Y. R. Chen, H. Z. Wu, and W. X. Liu, Philos. Mag. A **73**, 415 (1996).

[20] R. Osborn, N. H. Andersen, K. Clausen, M. A. Hackett, W. Hayes, M. T. Hutchings, and J. E. MacDonald, Mater. Sci. Forum **7**, 55 (1986); S. Hull, T. W. D. Farley, M. A. Hackett, W. Hayes, R. Osborn, N. H. Andersen, K. Clausen, M. T. Hutchings, and W. G. Stirling, Solid State Ionics **28-30**, 488 (1988).

[21] V. R. PaiVerneker, A. Petelin, F. J. Crowne, and D. C. Nagle, Phys. Rev. B **40**, 8555 (1989).

[22] P. Camagni, P. Galinetto, G. Samoggia, and N. Zema, Solid State Commun. **83**, 943 (1992).

[23] N. Nicoloso, A. Löbert, and B. Leibold, Sens. Actuators B **8**, 253 (1992).

[24] H. C. Wiemhofer, S. Harke, and U. Vohrer, Solid State Ionics **40/41**, 433 (1990).

[25] R. I. Merino and V. M. Orera, Solid State Ionics **76**, 97 (1995).

[26] R. I. Merino, V. M. Orera, E. E. Lomonova, and S. K. Batygov, Phys. Rev. B **52**, 6150 (1995).

[27] C. B. Azzoni, P. Camagni, G. Samoggia, and A. Paleari, Solid State Ionics **60**, 223 (1993); C. B. Azzoni and A. Paleari, Phys. Rev. B **40**, 9333 (1989).

[28] V. M. Orera, R. I. Merino, Y. Chen, R. Cases, and P. J. Alonso, Phys. Rev. B **42**, 9782 (1990).

[29] C. B. Azzoni and A. Paleari, Phys. Rev. B **44**, 6858 (1991).

[30] R. Ben-Michael, D. S. Tannhauser, and J. Genossar, Phys. Rev. B **43**, 7395 (1991).

[31] J. Shinar, D. S. Tannhauser, and B. L. Silver, Solid State Commun. **56**, 221 (1985).

[32] E. V. Stefanovich, A. L. Shluger, and C. R. A. Catlow, Phys. Rev. B **49**, 11 560 (1994).
[33] S. E. Kul'kova and O. N. Muryzhnikova, Physica B **192**, 284 (1993).
[34] A. B. Sobolev, A. N. Varaksin, O. A. Keda, and A. P. Khaĭmenov, Phys. Status Solidi B **162**, 165 (1990).
[35] G. A. Ol'khovic, I. I. Naumov, and O. I. Velikokhatnyi, J. Phys.: Condens. Matter **7**, 1273 (1995).
[36] Y. Chen, V. M. Orera, R. Gonzalez, R. T. Williams, G. P. Williams, G. H. Rozenblatt, and G. J. Pogatshnik, Phys. Rev. B **42**, 1410 (1990); B. Hederson, CRC Crit. Rev. Solid State Mater. Sci. **9**, 1 (1980).
[37] B. M. Klein *et al.*, Phys. Rev. B **35**, 5802 (1987).
[38] J. A. Marley and R. C. Dockerty, Phys. Rev. **140**, A304 (1965).
[39] A. Dwivedi and A. N. Cormack, Philos. Mag. A **61**, 1 (1990).
[40] W. C. Mackrodt and P. M. Woodrow, J. Am. Ceram. Soc. **69**, 277 (1986).
[41] V. Butler, C. R. A. Catlow, and B. E. F. Fender, Solid State Ionics **5**, 539 (1981).
[42] C. R. A. Catlow, A. V. Chadwick, A. N. Cormack, G. N. Greaves, G. V. Leslie, and L. M. Moroney, in *Defect Properties and Processing of High-Technology Nonmetallic Materials*, editec by Y. Chen *et al.*, MRS Symposia Proceedings No. 60 (Materials Research Society, Pittsburgh, 1986), p. 173.
[43] M. Wilson, U. Schönberger, and M. W. Finnis, Phys. Rev. B **54**, 9147 (1996).
[44] R. Orlando, C. Pisani, C. Roetti, and E. Stefanovich, Phys. Rev. B **45**, 592 (1992).
[45] H. J. F. Jansen, Phys. Rev. B **43**, 7267 (1991).
[46] F. Zandiehnadem, R. A. Murray, and W. Y. Ching, Physica B **150**, 19 (1988).
[47] R. H. French, S. J. Glass, F. S. Ohuchi, Y.-N. Xu, and W. Y. Ching, Phys. Rev. B **49**, 5133 (1994).
[48] L. Soriano, M. Abbate, J. Faber, C. Morant, and J. M. Sanz, Solid State Commun. **93**, 659 (1995).
[49] R. Car and M. Parrinello, Phys. Rev. Lett. **55**, 2471 (1985).
[50] We have used the code CPMD, version 3.0, developed by J. Hutter, P. Ballone, M. Bernasconi, P. Focher, E. Fois, S. Goedecker, M. Parrinello, and M. Tuckerman, at MPI für Festkörperforschung and IBM Zurich Research Laboratory (1990-1996).
[51] J. P. Perdew and A. Zunger, Phys. Rev. B **23**, 5048 (1981).
[52] N. Troullier and J. L. Martins, Phys. Rev. B **43**, 1993 (1991).
[53] H. J. Monkhorst and J. D. Pack, Phys. Rev. B **13**, 5188 (1976).
[54] C. Hartwigsen, S. Goedecker, and J. Hutter, Phys. Rev. B **58**, 3641 (1998).
[55] As reported in Ref. 54 the calculated bond length of the ZrO molecule is 3.235 Å by including the 4*s* and 4*p* states of Zr in the valence and 2.848 Å by freezing the 4*s* and 4*p* states in the core. The experimental ZrO bond length is 3.234 Å [K. P. Huber and G. Herzberg, *Constants of Diatomic Molecules* (Van Nostrand Reinhold, New York, 1979)].
[56] D. Vanderbilt, Phys. Rev. B **32**, 8412 (1985).
[57] W. H. Press, A. A. Teukolsky, W. T. Vetterling, and B. P. Flannery, *Numerical Recipes* (Cambridge University Press, Cambridge, 1992).
[58] B. H. O'Connor and T. M. Valentine, Acta Crystallogr., Sect. B: Struct. Crystallogr. Cryst. Chem. **25**, 2140 (1969); H. Ishibash, K. Shimomoto, and K. Nakahigashi, J. Phys. Chem. Solids **55**, 809 (1994); see also Ref. 87, Chap. 5, p. 5.
[59] S. Ikeda and K. Ogawa, J. Electron Microsc. **41**, 330 (1992).
[60] D. Murnaghan, Proc. Natl. Acad. Sci. USA **30**, 244 (1944).
[61] G. P. Francis and M. C. Payne, J. Phys.: Condens. Matter **2**, 4395 (1990).
[62] J. Adam and M. D. Rogers, Acta Crystallogr. **12**, 951 (1959); J. D. McCullough and K. N. Trueblood, *ibid.* **12**, 507 (1959); D. K. Smith and H. W. Newkirk, *ibid.* **18**, 983 (1965).
[63] G. Teufer, Acta Crystallogr. **15**, 1187 (1962).
[64] P. Aldebert and J. P. Traverse, J. Am. Ceram. Soc. **68**, 34 (1985).
[65] J. M. Léger, P. E. Tomaszewski, A. Atouf, and A. S. Pereira, Phys. Rev. B **47**, 14 075 (1993).
[66] L. Liu, J. Phys. Chem. Solids **41**, 331 (1980).
[67] L. M. Lityagina, S. S. Kabalkina, T. A. Pashkina, and A. I. Khzyainov, Sov. Phys. Solid State **20**, 2009 (1978).
[68] S. Desgreniers and K. Lagarec, in *Proceeding of the Joint XV AIRAPT & XXXIII EHPRG International Conference on High Pressure Science & Technology*, edited by W.A. Trzeciakowski (World Scientific, Singapore, 1996), p. 130.
[69] O. Ohtaka, T. Yamanaka, and T. Yagi, Phys. Rev. B **49**, 9295 (1994).
[70] H. Arashi, T. Yagi, S. Akimoto, and Y. Kudohi, Phys. Rev. B **41**, 4309 (1990); L. Liu, Earth Planet. Sci. Lett. **44**, 300 (1979), and reference therein.
[71] J. K. Dewhurst and J. E. Lowther, Phys. Rev. B **57**, 741 (1998).
[72] The transition pressure is given by the pressure at which the enthaply $H=E+PV$ of the two phases is equal. In a previous theoretical work on zirconia (Ref. 71) the transition pressure is erroneously computed by equating the energies and not the enthalpies of the two phases.
[73] A. De Vita, M. J. Gillan, J. S. Lin, M. C. Payne, I. Stich, and L. J. Clarke, Phys. Rev. B **46**, 12 964 (1992).
[74] The geometry optimization have been performed by using the Broyden-Fletcher-Goldfarb-Shanno algorithm (Ref. 57). For the sample A0 we also checked that the structure does not change by annealing at 1900 K for 1.3 ps.
[75] M. Filal, C. Petot, M. Mokchah, C. Chateau, and J. L. Carpentieri, Solid State Ionics **80**, 27 (1995); J. de Dios Solier, M. A. Pérez-Jubindo, A. Domiguez-Rodriguez, and A. H. Heuer, J. Am. Ceram. Soc. **72**, 1500 (1989).
[76] C.-K. Kwok and C. Rubin Aita, J. Appl. Phys. **66**, 2756 (1989).
[77] Y.-N. Xu, Z. Q. Gu, and W. Y. Ching, Phys. Rev. B **56**, 14 993 (1997).
[78] Ö. Ünal and M. Akinc, J. Am. Ceram. Soc. **79**, 805 (1996).
[79] W. R. Manning, O. Hunter, and B. R. Powell, J. Am. Ceram. Soc. **52**, 436 (1969).
[80] R. J. Ackermann, E. G. Rauh, and C. A. Alexander, High. Temp. Sci. **7**, 305 (1975).
[81] D. C. Bradley and P. Thornton, in *Comprehesive Inorganic Chemistry*, edited by J. P. Bailer, H. P. Emeléus, R. Nyholm, and A. F. Trotman-Dickenson (Pergamon, New York, 1973).
[82] H. M. Kandil, J. D. Greiner, and J. F. Smith, J. Am. Ceram. Soc. **67**, 341 (1984).
[83] R. P. Ingel and D. Lewis, J. Am. Ceram. Soc. **71**, 265 (1988).
[84] M. Fukuhara and I. Yamauchi, J. Mater. Sci. **28**, 4681 (1993).
[85] F. Frey, H. Boysen, and T. Vogt, Acta Crystallogr., Sect. B: Struct. Sci. **47**, 881 (1991).
[86] M. V. Nevitt, S.-K. Chan, J. Z. Liu, M. H. Grimsditch, and Y. Fang, Physica B **150**, 230 (1988).
[87] R. W. G. Wyckoff, *Crystal Structure* (Interscience, New York, 1966).
[88] O. Ohtaka, T. Yamanaka, S. Kume, N. Hara, H. Asano, and F. Izumi, Proc. Jpn. Acad., Ser. B: Phys. Biol. Sci. **66**, 193 (1990).